Device

Article

2D mixed halide perovskites for ultraviolet light-emitting diodes

Graphical abstract

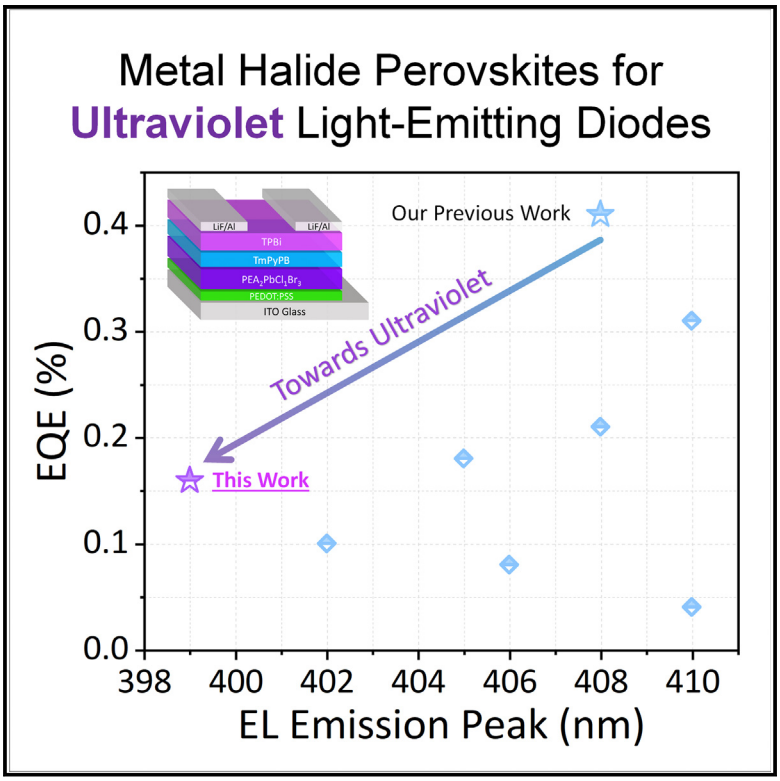

Highlights

- UV light-emitting diodes based on metal halide perovskites
- Precise tuning of the band gap in two-dimensional perovskite materials to 3.1 eV
- Dual-electron transport layer device stacks with electroluminescence at 399 nm
- Benchmark for external quantum efficiency (EQE) in this spectral range

Authors

Manchen Hu, Junrui Lyu, Natalia Murrietta, ..., Qi Zhou, Pournima Narayanan, Daniel N. Congreve

Correspondence

congreve@stanford.edu

In brief

This study showcases the advancement of perovskite light-emitting diodes (PeLEDs) into the ultraviolet range by fine-tuning halide compositions in two-dimensional perovskites. By optimizing the electron transport layer, we achieved high-purity electroluminescent emission at 399 nm, setting a new efficiency benchmark of 0.16%. These findings highlight the significant potential of large-band-gap perovskite materials for next-generation ultraviolet lighting technologies.

Hu et al., 2024, Device 2, 100511
November 15, 2024
https://doi.org/10.1016/j.device.2024.100511

CellPress

Please cite this article in press as: Hu et al., 2D mixed halide perovskites for ultraviolet light-emitting diodes, Device (2024), https://doi.org/10.1016/j.device.2024.100511

Device

CellPress
OPEN ACCESS

Article

2D mixed halide perovskites for ultraviolet light-emitting diodes

Manchen Hu,[1,3] Junrui Lyu,[1,3] Natalia Murrietta,[1,3] Sebastian Fernández,[1] William Michaels,[1] Qi Zhou,[1] Pournima Narayanan,[1,2] and Daniel N. Congreve[1,4,*]

[1]Department of Electrical Engineering, Stanford University, Stanford, CA 94305, USA
[2]Department of Chemistry, Stanford University, Stanford, CA 94305, USA
[3]These authors contributed equally
[4]Lead contact
*Correspondence: congreve@stanford.edu
https://doi.org/10.1016/j.device.2024.100511

THE BIGGER PICTURE Perovskite light-emitting diodes (PeLEDs) are quickly becoming top contenders for future display and lighting technologies. Recent advancements have pushed their emissive capabilities into the deep blue and violet regions, addressing a critical challenge in achieving shorter-emission wavelengths. By carefully engineering the materials and device structures, we have developed PeLEDs that emit at a wavelength of 399 nm, near ultraviolet (UV) light. This breakthrough not only simplifies the manufacturing process but also sets new efficiency records of PeLEDs in this color range. These findings highlight the significant potential of large-band-gap perovskite materials for next-generation UV lighting technologies.

SUMMARY

Advances in perovskite light-emitting diodes (PeLEDs) have established them as viable candidates for next-generation displays and lighting across the entire visible spectrum, with recent investigations extending their emissive properties into the deep blue and violet regions. However, achieving shorter emission wavelengths presents a significant challenge due to the larger band gaps required of both the perovskite and charge transport materials, compounding the difficulty in managing electron-hole pair recombination dynamics necessary for efficient electroluminescence. In this work, we precisely tune the halide composition in two-dimensional perovskites, successfully extending the band gap to 3.1 eV. By introducing an optimized dual-electron transport layer architecture, we improve electron injection and hole confinement within the perovskite matrix, culminating in a high-purity electroluminescent emission at 399 nm with a maximum external quantum efficiency of 0.16%, a benchmark for PeLEDs operating in this spectral domain. These findings highlight the potential of large-band-gap perovskite materials for next-generation light-emitting applications.

INTRODUCTION

Ultraviolet (UV) light, with its potent germicidal properties, is essential for sterilization in healthcare and food safety and drives advancements in data technology, three-dimensional (3D) printing, nanofabrication, and optical communication systems.[1–5] Despite its ubiquitous use, the development of UV light-emitting diode (LED) technology faces significant challenges, primarily dominated by the complex manufacturing processes associated with III-V semiconductors, including InGaN, GaN, and AlGaN materials.[1] These traditional methods rely on strict lattice matching and epitaxial growth, often necessitating the use of metal-organic chemical vapor deposition, which involves high-temperature toxic precursor gases.

The advent of metal halide perovskites and their extraordinary optoelectronic properties have revolutionized the field of LEDs.[2–10] These materials are celebrated for their ease of processing, tunable band gaps, high luminescence efficiency, and narrow emission linewidths, positioning perovskite LEDs (PeLEDs) as promising alternatives for display and lighting technologies. In less than a decade, PeLEDs have achieved external quantum efficiencies (EQEs) exceeding 25% for green and red emissions.[3,5,11–13] Additionally, blue PeLEDs, which demand larger-band-gap semiconductors, are on the cusp of achieving EQEs greater than 20%.[14–18]

Substantial progress has also been made in developing novel materials with wider band gaps, facilitating the transition toward deep blue and violet emission.[19–26] Jin et al. reported using the 2D perovskite 2-phenylethylammonium ($C_6H_5CH_2CH_2NH_3^+$, PEA) lead bromide (PEA_2PbBr_4) to achieve color-pure violet LEDs with 0.04% EQEs.[20] By adapting electric field deposition techniques, Jie et al. achieved deep blue LEDs with 0.31%

Please cite this article in press as: Hu et al., 2D mixed halide perovskites for ultraviolet light-emitting diodes, Device (2024), https://doi.org/10.1016/j.device.2024.100511

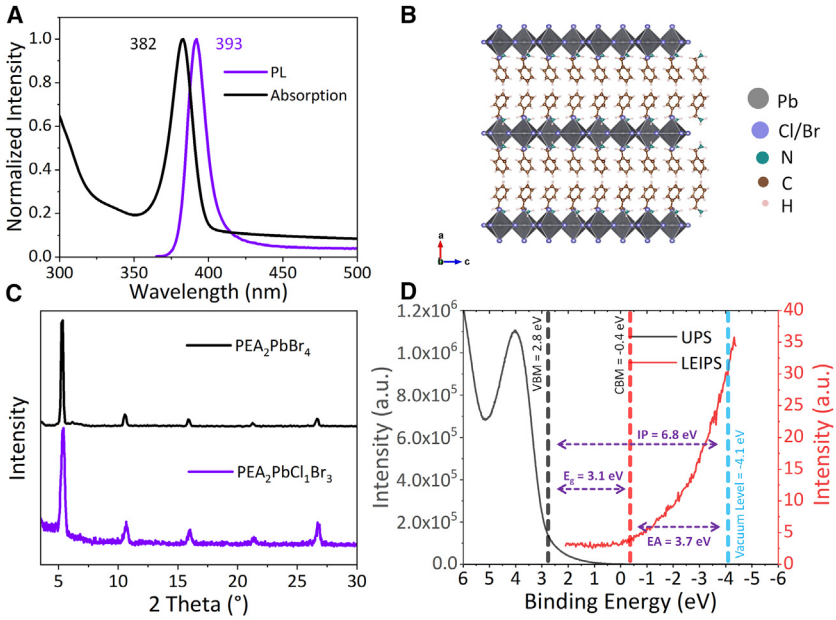

Figure 1. The optical and electronic properties of 2D perovskites

(A) The absorption spectrum and emission spectrum of the $PEA_2PbCl_1Br_3$ perovskite film under 330 nm excitation.

(B) Proposed crystal structure diagram of $PEA_2PbCl_1Br_3$.

(C) XRD pattern comparison of $PEA_2PbCl_1Br_3$ and PEA_2PbBr_4.

(D) UPS (black) and LEIPS (red) measurements of the $PEA_2PbCl_1Br_3$ perovskite film.

EQEs.[19] Besides 2D perovskites, 3D perovskite nanocrystals have also been explored for deep blue and violet devices. By synthesizing $CsPbCl_3$ nanocrystals with phenylphosphonic dichloride ($PhPOCl_2$), Qi et al. developed bright and stable $CsPbCl_3$ nanocrystals and fabricated violet LEDs with peak emission at 405 nm and 0.18% EQEs.[24] Regarding lead-free perovskites, Shan et al. synthesized $Cs_3Sb_2Br_9$ quantum dots and achieved violet LEDs with 0.21% EQEs.[21] Previously, our group improved the 2D perovskite crystallization process and produced violet LEDs with EQEs of 0.41% at 408 nm.[22]

Despite this progress, achieving solution-processed PeLEDs that can efficiently emit in the UV region has remained a challenging goal. The endeavor toward UV PeLEDs imposes even stricter requirements for larger band gaps in emissive perovskite materials and poses heightened challenges in the design of charge transport layers and the management of radiative recombination and energy transfer. In this work, we present PeLEDs based on a 2D perovskite, which achieves a single electroluminescence (EL) peak below 400 nm with a peak EQE of 0.16%. This effort not only validates the feasibility of UV PeLEDs but also provides device design rules to ensure color-pure and efficient perovskite light emission.

RESULTS

Demonstration of perovskite thin films with UV PL

Building on our previous work studying PEA_2PbBr_4 violet-emitting perovskites and taking advantage of the perovskites' tremendous halide tunability, we replaced 50% phenethylammonium bromide (PEABr) with phenethylammonium chloride (PEACl). The molar ratio of the perovskite precursors with PEACl, PEABr, and $PbBr_2$, respectively, in dimethyl sulfoxide (DMSO) was 1:1:1. The perovskite films were spin coated on quartz substrates and processed with a two-step annealing procedure according to our previous work.[22] More details can also be found in the experimental procedures section. The film shows a photoluminescent spectrum peak at 393 nm with approximately a 14 nm full width at half maximum (FWHM), which is shown in Figure 1A. The perovskite films also have a strong excitonic band absorption peak at 382 nm, similar to the pure bromide 2D perovskite PEA_2PbBr_4 with an absorption peak of 402 nm.[22] According to the feed ratio, we denote our new perovskite as $PEA_2PbCl_1Br_3$. As shown in Figure 1B, we believe that $PEA_2PbCl_1Br_3$ should possess a 2D structure similar to that of PEA_2PbBr_4, where the $[PbX_6]$ (X = Cl or Br) octahedral layers are interspersed with organic PEA layers. This 2D structure is supported by X-ray diffraction (XRD) measurements. The XRD patterns in Figure 1C confirm that $PEA_2PbCl_1Br_3$ has a similar 2D structure to PEA_2PbBr_4, denoted by the signature (*00l*) peaks. We also performed XRD fine scans from 4.8° to 5.8° and from 15.4° to 16.4° to enable detailed comparisons between $PEA_2PbCl_1Br_3$ and PEA_2PbBr_4. No obvious peak shifts are observed in these two XRD spectra (shown in Figures S1A and S1B). Considering only a small portion of Br is substituted by Cl, this partial substitution may not be sufficient to cause a noticeable change in the crystal structures as observed through XRD.

To further investigate the chemical composition of the perovskite films, X-ray photoelectron spectroscopy (XPS) was employed to discern the precise atomic ratio of chlorine to bromine. As depicted in Figure S2A, the XPS spectrum allows us to elucidate the elemental constitution of the films. Furthermore, Figures S2B and S2C offer a detailed look at the binding energy regions corresponding to Pb 4f, Cl 2p, and Br 3p, respectively. Analyses of these spectra reveal that the atomic ratio within the as-synthesized perovskite films stands at Pb:Cl:Br = 21.8:17.3:60.9. This ratio aligns well with the intended stoichiometric feed ratio of Pb:Cl:Br = 1:1:3, confirming the accuracy of our fabrication process in achieving the desired chemical composition.

Emissive defect states, which are particularly prone to forming within large-band-gap semiconductors, can detrimentally affect the performance of LEDs. The presence of defect states in semiconductors often manifests as changes in the PL spectrum upon varying the excitation wavelength. Figure S3 demonstrates the photoluminescence (PL) spectra of perovskite films under excitation wavelengths ranging from 260 to 360 nm. Notably, the

Please cite this article in press as: Hu et al., 2D mixed halide perovskites for ultraviolet light-emitting diodes, Device (2024), https://doi.org/10.1016/j.device.2024.100511

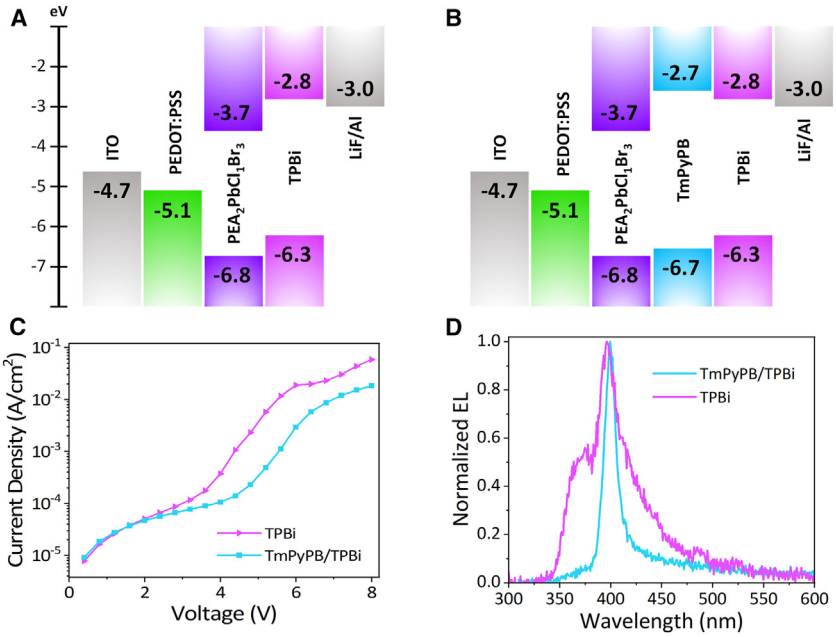

Figure 2. LED devices with different architectures

(A) Energy-level diagram of the single-ETL device (i.e., TPBi device).

(B) Energy-level diagram of the dual-ETL device (i.e., TmPyPB/TPBi device).

(C) J-V curves for the TPBi and TmPyPB/TPBi devices.

(D) EL spectra of the TPBi and TmPyPB/TPBi devices show pure emission from the dual-ETL architecture.

consistency of the PL spectra across these excitation wavelengths suggests that $PEA_2PbCl_1Br_3$ exhibits solely band-to-band emission without significant additional radiative states. Moreover, there is only a minor contribution from red-shifted self-trapped excitons (STEs) to the PL emission. Given that $[PbCl_6]$-based perovskites are known for their broad white emission stemming from STEs,[27–29] the absence of broad emission in $PEA_2PbCl_1Br_3$ could be attributed to the predominance of bromide in the $[PbX_6]$ octahedral sites, as our synthesis involved a lower proportion of chloride substitution. This clarity in the PL spectra underscores the potential of $PEA_2PbCl_1Br_3$ as a promising candidate for UV EL applications. It should be noted that due to the relatively low PL quantum yield (PLQY) of $PEA_2PbCl_1Br_3$ (we previously measured a value of 8% for PEA_2PbBr_4)[22] and the low sensitivity of our integrating sphere in the UV wavelength region, we could not resolve accurate PLQY values of the UV films. We estimate that the PLQY is on the order of 1%.

To ascertain the precise energy levels of the organic-inorganic hybrid 2D perovskites, we employed UV photoelectron spectroscopy (UPS) and low-energy inverse photoelectron spectroscopy (LEIPS) to probe the ionization potential (IP) and electron affinity (EA), respectively. LEIPS is particularly advantageous for its minimal chemical degradation impact on organic constituents, rendering it an optimal technique for assessing the unoccupied conduction band of organic semiconductors.[30,31] As depicted in Figure 1D, the IP was determined to be 6.8 eV using UPS. Concurrently, LEIPS facilitated the measurement of UV light emission from our sample upon exposure to low-energy electrons, enabling the calculation of an EA of 3.7 eV. Comprehensive details and calculations are presented in the supplemental information (see Figures S4 and S5 and Notes S1 and S2). Consequently, the band gap of the perovskite was calculated to be 3.1 eV, corroborating the emission and absorption data presented in Figure 1A.

Investigation on dual ETLs

Traditional deep blue and violet PeLEDs often employ 2,2′,2″-(1,3,5-benzinetriyl)-tris(1-phenyl-1H-benzimidazole) (TPBi) as the electron transport layer (ETL) due to its favorable electronic properties.[19,20,22,25,32–35] However, as shown by the energy-level diagram in Figure 2A, TPBi's highest occupied molecular orbital (HOMO) is positioned at a higher energy compared to the valence band maximum of $PEA_2PbCl_1Br_3$. This mismatch hinders effective hole confinement within the perovskite layer, potentially facilitating hole leakage and non-radiative recombination processes. Moreover, the band gap of TPBi, approximately 3.5 eV, is very close to the perovskite band gap of 3.1 eV, raising concerns over emission spectral purity. The violet curve in Figure 2D illustrates the EL spectrum of a $PEA_2PbCl_1Br_3$ device with a traditional TPBi structure. When contrasted with the EL spectrum from a TPBi-only (no perovskite) device (Figure S6), notable emission from the TPBi layer is observed, indicating excitonic recombination within TPBi that detracts from the desired device performance. We suspect that the small peak around 480 nm results from old chemical residues inside our general-use evaporator, which introduce unintended emission centers.

To address this challenge, we integrated an additional ETL, 1,3,5-tri(*m*-pyridin-3-ylphenyl)benzene (TmPyPB), between the perovskite and TPBi layers. TmPyPB, known for its electron-deficient pyridine moieties, serves as an effective electron-transport and hole-blocking layer in various organic electronic devices.[36–41] Its lower HOMO level of 6.7 eV is compatible with the valence band maximum of $PEA_2PbCl_1Br_3$, thereby enhancing hole-blocking efficiency within the dual-ETL device stack. Furthermore, TmPyPB's wider band gap of 4.0 eV mitigates the spectral overlap with the perovskite emission. For the modified device architecture, we employed a dual-layer ETL comprising 20 nm TmPyPB and 20 nm TPBi, as shown in Figure 2B, as compared to 40 nm TPBi in Figure 2A. The device architecture in Figure 2B led to a considerable reduction in current density at operational voltages, as evidenced by the current density measurements in Figure 2C; at 5 V, the TmPyPB/TPBi device exhibited a current density of an order of magnitude lower than that of the TPBi device. It is worth noting that dual-ETL devices have better band alignment, leading to smaller currents after turn on compared to single-ETL devices.[42,43] However, TmPyPB is also not perfect, as the higher HOMO level of

Please cite this article in press as: Hu et al., 2D mixed halide perovskites for ultraviolet light-emitting diodes, Device (2024), https://doi.org/10.1016/j.device.2024.100511

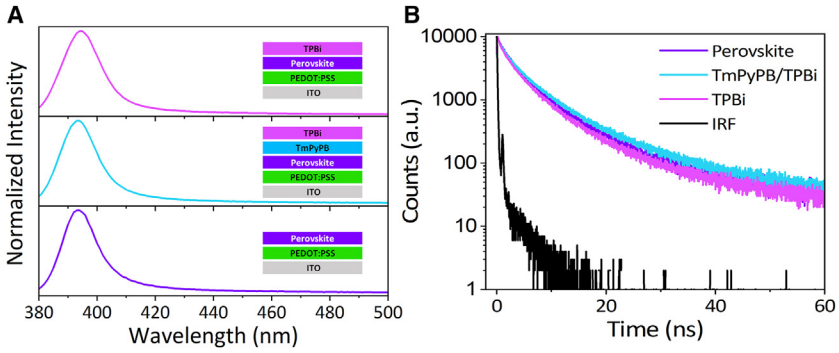

Figure 3. Optical measurements for three different device architectures

(A) PL spectra of perovskites with different ETLs. The insets show the diagrams of the measured samples.

(B) Time-resolved photoluminescence decay curves of perovskites with different ETLs.

TmPyPB compared to the valence band maximum of $PEA_2PbCl_1Br_3$ can lead to hole leakage. Devices with TmPyPB only as the ETL performed substantially worse. Its higher lowest unoccupied molecular orbital level compared to TPBi introduces a higher energy barrier for electron injection, which correlates with the increased turn-on voltage observed in the dual-ETL LED (~5.2 V, Figure 4C) compared to the single-ETL (TPBi) LED (~4.4 V, Figure S7). Further optimization of the hole transport layers and alignment of energy levels is necessary to further improve device performance.[44]

The EL spectra depicted in Figure 2D reveal that the TmPyPB/TPBi device produces a sharp perovskite emission peak at 399 nm. In contrast, the EL spectra of devices with only TPBi ETLs show broader peaks, indicating recombination occurring both in the perovskite and TPBi layers. This broader spectrum matches well with the perovskite emission (Figure 1A) and the TPBi emission (Figure S6). The strategic replacement of part of the TPBi layer with TmPyPB effectively suppresses exciton formation in the TPBi layer and promotes exciton recombination within the perovskite layer, culminating in the observed clean, single-peak EL emission.

Optical measurements were also employed to further analyze the influence of different device architectures on the optical properties of the perovskite. As depicted in Figure 3A, three distinct device structures—ITO/poly(3,4-ethylenedioxythiophene)polystyrene sulfonate (PEDOT:PSS)/perovskite, ITO/PEDOT:PSS/perovskite/TmPyPB/TPBi, and ITO/PEDOT:PSS/perovskite/TPBi—exhibited identical PL spectra when excited with a 365 nm lamp. To delve deeper, time-resolved PL (TRPL) was conducted using a 379 nm pulsed laser to excite the devices, where the 393 nm emission was monitored. Note that TPBi PL was not observed under 365 or 379 nm excitations. The TRPL data, presented in Figure 3B alongside the instrument response function, were modeled using a bi-exponential decay function:

$$I(t) = A_1 \exp\left(-\frac{t}{\tau_1}\right) + A_2 \exp\left(-\frac{t}{\tau_2}\right)$$

where A_1 and A_2 are the amplitudes for the PL decay times of τ_1 and τ_2. $I(t)$ is the intensity of the PL. The fitted parameters are summarized in Table 1. The PL decay of the perovskite/TPBi sample had a relatively short average PL lifetime (τ_{ave} = 3.28 ns) compared with the perovskite-only sample (τ_{ave} = 3.76 ns), indicating that TPBi introduced luminescence quenching for the perovskite. The perovskite/TmPyPB/TPBi sample, however, showed the longest PL lifetime (τ_{ave} = 4.04 ns) among the three samples in Table 1, implying that TmPyPB is more effective in mitigating non-radiative recombination, potentially due to its energy-level alignment with the perovskite, which helps to confine charge carriers within the perovskite layer.

Evaluation of UV PeLED performance

Finally, we fabricated a series of dual-ETL PeLEDs with the structure quartz/ITO/PEDOT:PSS/$PEA_2PbCl_1Br_3$/TmPyPB/TPBi/LiF/Al, as shown in Figure 4A. Scanning electron microscopy (SEM) of the cross-section of the device is shown in Figure S8. PEDOT:PSS was spin coated on quartz ITO substrates, and the perovskite was spin coated on top of PEDOT:PSS. The substrates were then transferred to a vacuum chamber for thermal evaporation, where 20 nm of TmPyPB, 20 nm of TPBi, 2 nm of LiF, and 100 nm of Al were thermally evaporated sequentially. More fabrication details can be found in the experimental procedures section. According to the previous two-step annealing procedure, we can also obtain 2D perovskite thin films with good coverage and crystallization, which is shown in the atomic force microscopy (AFM) images in Figure S9.

The EQE-current density curves and the current density-voltage-radiance curves of our champion devices are shown in Figures 4B and 4C. Our dual-ETL PeLEDs achieve a peak EQE of 0.16% at 2.9 mA/cm^2, with an average EQE of 0.08% over 58 devices (Figure S10). At voltages >5.2 V, the device turned on and reached its maximum radiance of 33 mWsr^{-1}m^{-2} at 7.2 V. We did not observe any major change in the EL spectra across a range of operating voltages from 6 to 8 V, with only a small shoulder visible at 6 V. At 6 V, the electric field across the PeLEDs may not be strong enough for electrons to overcome the energetic barriers at the interfaces, effectively leading to excitons forming in TPBi.

As shown in Figure 4D, the EL shows a dominant peak at 399 nm with an FWHM of 14 nm. We also conducted a detailed analysis of the EL spectra of devices over time, employing a constant current bias of 10 mA/cm^2 in an ambient atmosphere. The results, depicted in Figure S11A, show that the EL spectra remain stable throughout the measurement duration, indicating consistent emission characteristics under the given operational conditions. However, a critical aspect noted in our observations is the limitation of the device's operational lifetime, as is evident from the T_{50} value being less than 1 s (refer to Figure S11B).

The degradation of our UV PeLED is more severe than that in red, green, and blue PeLEDs.[45] Higher operational voltages in

Please cite this article in press as: Hu et al., 2D mixed halide perovskites for ultraviolet light-emitting diodes, Device (2024), https://doi.org/10.1016/j.device.2024.100511

Table 1. Summary of fitted parameters for TRPL measurements

Materials	A_1 (%)	τ_1, ns	A_2 (%)	τ_2, ns	R-squared, %	τ_{ave}, ns
Perovskite	5,319.7 (52.4)	1.60	4,829.8 (47.6)	6.14	99.90	3.76
Perovskite/TmPyPB/TPBi	5,128.3 (52.2)	1.55	4,701.6 (47.8)	6.75	99.89	4.04
Perovskite/TPBi	5,349.5 (51.6)	1.21	5,025.3 (48.4)	5.48	99.88	3.28

UV PeLEDs result in increased electric fields, accelerating ion migration within the perovskite layer. This ion movement creates defects and vacancies, leading to non-radiative recombination centers that diminish device efficiency and lifetime. Additionally, the large band gap of UV-emitting perovskites necessitates higher turn-on voltages, which contribute to greater electrical stress and the breaking down of material. This stress can cause lattice strain and deformation, disrupting the crystal structure and degrading material quality. Furthermore, high-energy UV photons could potentially break chemical bonds within the organics, leading to photodegradation and the formation of trap states, which further reduce device performance and stability. In summary, the higher band gap and associated stresses in UV-emitting 2D perovskites result in pronounced instability issues, necessitating advanced mitigation strategies to enhance device longevity.

Figure 5 presents a comprehensive overview of the performance benchmarks for solution-processed lead-halide violet PeLEDs reported to date. This work demonstrates the emergence of emissive perovskites for the UV regime, highlighting the potential of wide-band-gap perovskite materials. Notably, this advancement also delivers an EQE that is highly competitive with the best-performing violet-emitting PeLEDs.

Conclusions

This investigation into the optoelectronic properties of the mixed halide 2D perovskite material $PEA_2PbCl_1Br_3$ has yielded significant insights into the complex mechanisms governing its performance in PeLEDs. The introduction of TmPyPB as an additional ETL enhances charge carrier confinement and reduces non-radiative losses, as evidenced by both optical measurements and electronic device analysis. Our work culminates in the successful demonstration of solution-processed PeLEDs with UV emission below 400 nm, surpassing the spectral limitations of previously reported devices while achieving reasonable EQE values. These findings not only highlight the potential of 2D perovskites in next-generation optoelectronics but also pave the way for further exploration into novel device architectures and material compositions, with the ultimate goal of realizing highly efficient, stable, and commercially viable UV electroluminescent devices.

EXPERIMENTAL PROCEDURES

Resource availability

Lead contact

Further information and requests for resources and materials should be directed to and will be fulfilled by the lead contact, Daniel N. Congreve (congreve@stanford.edu).

Materials availability

All commercially available starting reagents and solvents were used directly without further treatment unless otherwise specified.

Data and code availability

The published article includes all data analyzed in this study. Data are available from the lead contact upon reasonable request.

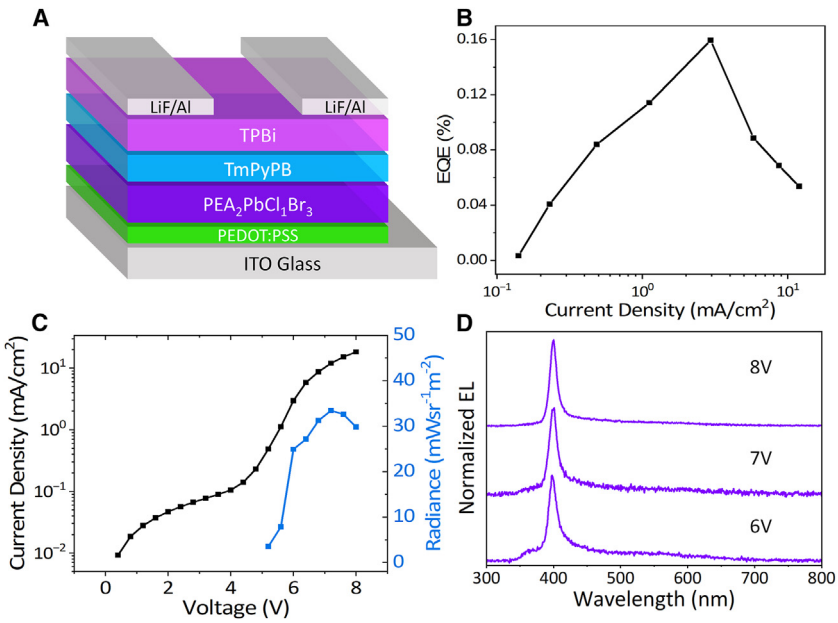

Figure 4. Dual-ETL PeLED performance

(A) Cross-section diagram of the dual-ETL PeLEDs.

(B) EQE-current density characteristics of the champion dual-ETL PeLED.

(C) Current density-voltage-radiance characteristics of the champion dual-ETL PeLED.

(D) EL spectra under different operating voltages.

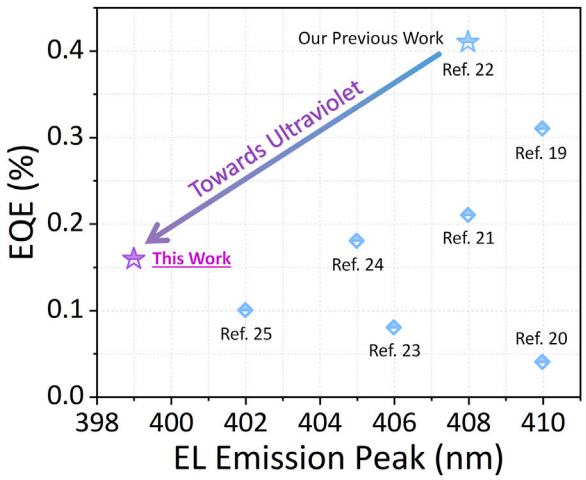

Figure 5. Summary of solution-processed lead-halide PeLEDs in the violet and ultraviolet regions

Materials

PEACl (>98%), PEABr (>98%), and lead(II) bromide ($PbBr_2$; >99.999%) were purchased from Sigma-Aldrich. Anhydrous DMSO (≥99.9%), anhydrous N,N-dimethylformamide (DMF; 99.8%), and anhydrous lithium fluoride (LiF, ≥99.99%) were purchased from Sigma-Aldrich. PEDOT:PSS (Clevios Al 4083) was purchased from Heraeus. TPBi (>99.5%) and TmPyPB (>99.5%) were purchased from Ossila. Al (99.99%) pellets were purchased from Kurt J. Lesker Company. All chemicals were used directly as received.

Perovskite precursor

The perovskite precursor preparation was conducted inside a nitrogen-filled glovebox at room temperature. 0.1 M $PEA_2PbCl_1Br_3$ stock solution was prepared by dissolving stoichiometric PEACl, PEABr, and $PbBr_2$ in DMSO and then left under continuous stirring for 2 h. The precursor solution was then filtered with a 0.22 μm PTFE syringe filter before spin coating.

PeLED fabrication

The patterned-ITO-coated quartz substrates (ITO resistance: 20 Ω/square, Qingdao Vatti Glass) were sequentially solvent cleaned via sonication in ultra-pure water (Millipore Sigma MilliQ Ultrapure Water Purification System) with a 2% volume of detergent (Hellmanex III), acetone, and isopropanol for 15 min, respectively. These substrates were then dried under compressed air and treated with UV ozone for 15 min (Jelight UV-Ozone Cleaner) immediately before spin coating PEDOT:PSS. The PEDOT:PSS aqueous solution was filtered with a 0.22 μm PVDF syringe filter and then spin coated onto the cleaned ITO substrates at 4,000 rpm for 60 s (with a ramp of 2,000 rpm/s), followed by annealing at 150°C for 20 min in ambient air. Next, the substrates were transferred to a nitrogen-filled glovebox. After the substrates cooled down to room temperature, 150 μL perovskite precursor was dropped onto the PEDOT:PSS film and spin coated at 3,000 rpm with a ramp of 2,000 rpm/s for 30 s. Subsequently, the substrates were transferred to a glass Petri dish containing 30 μL of DMF vapor for 60 s. The DMF-treated Petri dish had a resting period of 5 min between each substrate to ensure a DMF vapor-rich environment. The Petri dish was wiped down with a dry nylon wipe before adding 30 μL of new DMF between spins. Afterward, the substrates were annealed at 70°C for 5 min in a nitrogen atmosphere to remove any residual solvent. After the substrates cooled down to room temperature, they were moved into a high-vacuum thermal evaporation chamber housed within a nitrogen-filled glovebox, where TmPyPB (20 nm), TPBi (20 nm), LiF (2 nm), and Al (100 nm) were deposited at 2, 1.5, 0.1, and 3 Å/s, respectively, under a high vacuum of approximately 8×10^{-6} mbar. The device area for all devices was 0.04 cm^2, as defined by the overlapping area of the ITO and Al electrode.

The perovskite device with a single TPBi ETL (Figure 2A) was fabricated using the above methods. However, 40 nm of TPBi was deposited, replacing the 20 nm of TmPyPB. The TPBi EL device (Figure S6) was fabricated using the same PEDOT:PSS deposition techniques, and subsequently, 40 nm of TPBi replaced the original TmPyPB/TPBi layer. No perovskite layer was deposited.

Device characterization

EL spectra were captured using an Ocean Insight QE Pro with voltages sourced to the device from a pre-programmed Keithley 2400. Currrent density - voltage - radiance characterizations from 0 to 10 V with a voltage scanning step of 0.4 V were performed using an HP4145A and a calibrated Thorlabs photodiode (FDS1010-CAL) mounted just above the face of the device.

Structure and optical characterizations

The AFM images were taken in ambient air by Bruker Dimension Icon ScanAsyst with PeakForce mode. The SEM images were collected on an FEI Magellan 400 XHR scanning electron microscope operating at 5 kV, 25 pA below 9×10^{-5} mbar with UC mode. The XRD data were collected using a PANalytical X'Pert PRO XRD system with Cu Ka radiation. The XPS data were collected using XPS: PHI VersaProbe 4 with a monochromatized Al (Ka) source and dual-gun neutralizing system. UPS spectra were collected inside PHI VersaProbe 4 with an incident light energy of 21.22 eV (He I source). A bias of −10 V was applied to the sample to measure the secondary electron cutoff energy. Spectra both with and without bias were obtained. LEIPS was also conducted inside PHI VersaProbe 4 with an electron gun with a band-pass filter of 4.77 eV. Low-energy-electron transmission (LEET) spectra were simultaneously collected using a microcurrent meter. The PL spectra were measured with a Horiba FluoroLog-3 system with a Xe arc lamp. The PL lifetimes were measured with the same system but with a pulsed 375 nm laser. The absorption spectra were collected on the Agilent Cary 6000i UV-Vis-NIR system with transmission mode.

SUPPLEMENTAL INFORMATION

Supplemental information can be found online at https://doi.org/10.1016/j.device.2024.100511.

ACKNOWLEDGMENTS

A portion of this work was performed at the Stanford Nano Shared Facilities (SNSF), supported by the National Science Foundation under award ECCS-2026822. We thank Juliet Jamtgaard for her assistance with the measurements conducted using the PHI VersaProbe 4 and for discussions about the data analysis. M.H., J.L., N.M., and Q.Z. acknowledge the support of the Department of Electrical Engineering at Stanford University. N.M. and W.M. acknowledge the support of Research Experience for Undergraduates (REU) Program at the Department of Electrical Engineering, Stanford University. P.N. acknowledges the support of a Stanford Graduate Fellowship in Science & Engineering (SGF) as a Gabilan Fellow and the Chevron Fellowship in Energy. S.F. acknowledges the support from Stanford University as a Diversifying Academia, Recruiting Excellence (DARE) Fellow, the US Department of Energy (DOE) Building Technologies Office (BTO) as an IBUILD Graduate Research Fellow, the Stanford Graduate Fellowship in Science & Engineering (SGF) as a P. Michael Farmwald Fellow, and the National GEM Consortium as a GEM Fellow. This work was performed under an appointment to the Building Technologies Office (BTO) IBUILD Graduate Research Fellowship administered by the Oak Ridge Institute for Science and Education (ORISE) and managed by Oak Ridge National Laboratory (ORNL) for the DOE. ORISE is managed by Oak Ridge Associated Universities (ORAU). All opinions expressed in this paper are the authors' and do not necessarily reflect the policies and views of the DOE, EERE, BTO, ORISE, ORAU, or ORNL.

AUTHOR CONTRIBUTIONS

M.H., J.L., and N.M. designed and performed experiments, analyzed data, and wrote the manuscript. S.F. and W.M. assisted in EQE measurements. Q.Z. and

P.N. assisted in the optical characterization of thin films. D.N.C. guided the research. All authors contributed to the manuscript.

DECLARATION OF INTERESTS

D.N.C. is a co-founder of and chief scientific advisor to Quadratic 3D, Inc.

Received: May 3, 2024
Revised: July 6, 2024
Accepted: July 19, 2024
Published: August 21, 2024

REFERENCES

1. Amano, H., Collazo, R., Santi, C.D., Einfeldt, S., Funato, M., Glaab, J., Hagedorn, S., Hirano, A., Hirayama, H., Ishii, R., et al. (2020). The 2020 UV emitter roadmap. J. Phys. D Appl. Phys. *53*, 503001. https://doi.org/10.1088/1361-6463/ABA64C.
2. Fakharuddin, A., Gangishetty, M.K., Abdi-Jalebi, M., Chin, S.H., bin Mohd Yusoff, A.R., Congreve, D.N., Tress, W., Deschler, F., Vasilopoulou, M., and Bolink, H.J. (2022). Perovskite light-emitting diodes. Nat. Electron. *5*, 203–216. https://doi.org/10.1038/s41928-022-00745-7.
3. Tan, Z.K., Moghaddam, R.S., Lai, M.L., Docampo, P., Higler, R., Deschler, F., Price, M., Sadhanala, A., Pazos, L.M., Credgington, D., et al. (2014). Bright light-emitting diodes based on organometal halide perovskite. Nat. Nanotechnol. *9*, 687–692. https://doi.org/10.1038/nnano.2014.149.
4. Yang, D., Zhao, B., Yang, T., Lai, R., Lan, D., Friend, R.H., Di, D., Yang, D., Zhao, B., Lai, R., et al. (2022). Toward Stable and Efficient Perovskite Light-Emitting Diodes. Adv. Funct. Mater. *32*, 2109495. https://doi.org/10.1002/ADFM.202109495.
5. Song, J., Li, J., Li, X., Xu, L., Dong, Y., Zeng, H., Song, J., Li, J., Li, X., Xu, L., et al. (2015). Quantum Dot Light-Emitting Diodes Based on Inorganic Perovskite Cesium Lead Halides (CsPbX3). Adv. Mater. *27*, 7162–7167. https://doi.org/10.1002/ADMA.201502567.
6. Li, J., Du, P., Guo, Q., Sun, L., Shen, Z., Zhu, J., Dong, C., Wang, L., Zhang, X., Li, L., et al. (2023). Efficient all-thermally evaporated perovskite light-emitting diodes for active-matrix displays. Nat. Photonics *17*, 435–441. https://doi.org/10.1038/s41566-023-01177-1.
7. Kim, J.S., Heo, J.M., Park, G.S., Woo, S.J., Cho, C., Yun, H.J., Kim, D.H., Park, J., Lee, S.C., Park, S.H., et al. (2022). Ultra-bright, efficient and stable perovskite light-emitting diodes. Nature *611*, 688–694. https://doi.org/10.1038/s41586-022-05304-w.
8. Cho, H., Jeong, S.H., Park, M.H., Kim, Y.H., Wolf, C., Lee, C.L., Heo, J.H., Sadhanala, A., Myoung, N., Yoo, S., et al. (2015). Overcoming the electroluminescence efficiency limitations of perovskite light-emitting diodes. Science *350*, 1222–1225. https://doi.org/10.1126/SCIENCE.AAD1818/SUPPL_FILE/CHO.SM.PDF.
9. Fernández, S., Michaels, W., Hu, M., Narayanan, P., Murrietta, N., Gallegos, A.O., Ahmed, G.H., Lyu, J., Gangishetty, M.K., and Congreve, D.N. (2023). Trade-off between efficiency and stability in Mn2+-doped perovskite light-emitting diodes. Device *1*, 100017. https://doi.org/10.1016/j.device.2023.100017.
10. Zhang, J., Cai, B., Zhou, X., Yuan, F., Yin, C., Wang, H., Chen, H., Ji, X., Liang, X., Shen, C., et al. (2023). Ligand-Induced Cation–π Interactions Enable High-Efficiency, Bright, and Spectrally Stable Rec. 2020 Pure-Red Perovskite Light-Emitting Diodes. Adv. Mater. *35*, 2303938. https://doi.org/10.1002/ADMA.202303938.
11. Kim, Y.H., Kim, S., Kakekhani, A., Park, J., Park, J., Lee, Y.H., Xu, H., Nagane, S., Wexler, R.B., Kim, D.H., et al. (2021). Comprehensive defect suppression in perovskite nanocrystals for high-efficiency light-emitting diodes. Nat. Photonics *15*, 148–155. https://doi.org/10.1038/s41566-020-00732-4.
12. Jiang, J., Chu, Z., Yin, Z., Li, J., Yang, Y., Chen, J., Wu, J., You, J., Zhang, X., Jiang, J., et al. (2022). Red Perovskite Light-Emitting Diodes with Efficiency Exceeding 25% Realized by Co-Spacer Cations. Adv. Mater. *34*, 2204460. https://doi.org/10.1002/ADMA.202204460.
13. Bai, W., Xuan, T., Zhao, H., Dong, H., Cheng, X., Wang, L., Xie, R.-J., Bai, W., Xuan, T., Zhao, H., et al. (2023). Perovskite Light-Emitting Diodes with an External Quantum Efficiency Exceeding 30. Adv. Mater. *35*, 2302283. https://doi.org/10.1002/ADMA.202302283.
14. Zhou, W., Shen, Y., Cao, L.X., Lu, Y., Tang, Y.Y., Zhang, K., Ren, H., Xie, F.M., Li, Y.Q., and Tang, J.X. (2023). Manipulating Ionic Behavior with Bifunctional Additives for Efficient Sky-Blue Perovskite Light-Emitting Diodes. Adv. Funct. Mater. *33*, 2301425. https://doi.org/10.1002/ADFM.202301425.
15. Liu, B., Li, J., Wang, G., Ye, F., Yan, H., Zhang, M., Dong, S.C., Lu, L., Huang, P., He, T., et al. (2022). Lattice strain modulation toward efficient blue perovskite light-emitting diodes. Sci. Adv. *8*, 138. https://doi.org/10.1126/SCIADV.ABQ0138/SUPPL_FILE/SCIADV.ABQ0138_SM.PDF.
16. Chu, S., Zhang, Y., Xiao, P., Chen, W., Tang, R., Shao, Y., Chen, T., Zhang, X., Liu, F., and Xiao, Z. (2022). Large-Area and Efficient Sky-Blue Perovskite Light-Emitting Diodes via Blade-Coating. Adv. Mater. *34*, 2108939. https://doi.org/10.1002/ADMA.202108939.
17. Xing, J., Zhao, Y., Askerka, M., Quan, L.N., Gong, X., Zhao, W., Zhao, J., Tan, H., Long, G., Gao, L., et al. (2018). Color-stable highly luminescent sky-blue perovskite light-emitting diodes. Nat. Commun. *9*, 3541. https://doi.org/10.1038/s41467-018-05909-8.
18. Jiang, Y., Qin, C., Cui, M., He, T., Liu, K., Huang, Y., Luo, M., Zhang, L., Xu, H., Li, S., et al. (2019). Spectra stable blue perovskite light-emitting diodes. Nat. Commun. *10*, 1868. https://doi.org/10.1038/s41467-019-09794-7.
19. Deng, W., Jin, X., Lv, Y., Zhang, X., Zhang, X., Jie, J., Deng, W., Jin, X.C., Lv, Y., Zhang, X.J., et al. (2019). 2D Ruddlesden–Popper Perovskite Nanoplate Based Deep-Blue Light-Emitting Diodes for Light Communication. Adv. Funct. Mater. *29*, 1903861. https://doi.org/10.1002/ADFM.201903861.
20. Liang, D., Peng, Y., Fu, Y., Shearer, M.J., Zhang, J., Zhai, J., Zhang, Y., Hamers, R.J., Andrew, T.L., and Jin, S. (2016). Color-Pure Violet-Light-Emitting Diodes Based on Layered Lead Halide Perovskite Nanoplates. ACS Nano *10*, 6897–6904. https://doi.org/10.1021/ACSNANO.6B02683/ASSET/IMAGES/LARGE/NN-2016-026833_0005.JPEG.
21. Ma, Z., Shi, Z., Yang, D., Zhang, F., Li, S., Wang, L., Wu, D., Zhang, Y., Na, G., Zhang, L., et al. (2020). Electrically-Driven Violet Light-Emitting Devices Based on Highly Stable Lead-Free Perovskite Cs3Sb2Br9 Quantum Dots. ACS Energy Lett. *5*, 385–394. https://doi.org/10.1021/ACSENERGYLETT.9B02096/ASSET/IMAGES/LARGE/NZ9B02096_0005.JPEG.
22. Hu, M., Fernández, S., Zhou, Q., Narayanan, P., Saini, B., Schloemer, T.H., Lyu, J., Gallegos, A.O., Ahmed, G.H., and Congreve, D.N. (2023). Water additives improve the efficiency of violet perovskite light-emitting diodes. Matter *6*, 2356–2367. https://doi.org/10.1016/J.MATT.2023.05.018.
23. Chu, Z., Chen, H., Mao, X., Tajima, D., Koshimizu, M., Fujimoto, Y., Ma, L., Wang, C., and Chu, Y. (2023). Centimeter-Scale Violet Light Emitting Diode with Two-Dimensional BA2PbBr4 Perovskite Emitter. J. Electrochem. Soc. *170*, 065501. https://doi.org/10.1149/1945-7111/ACD811.
24. Zhang, C., Wan, Q., Ono, L.K., Liu, Y., Zheng, W., Zhang, Q., Liu, M., Kong, L., Li, L., and Qi, Y. (2021). Narrow-Band Violet-Light-Emitting Diodes Based on Stable Cesium Lead Chloride Perovskite Nanocrystals. ACS Energy Lett. *6*, 3545–3554. https://doi.org/10.1021/ACSENERGYLETT.1C01380/ASSET/IMAGES/LARGE/NZ1C01380_0004.JPEG.
25. Hu, Q., Guo, J., Lu, M., Lu, P., Zhang, Y., Yu, W.W., and Bai, X. (2021). Efficient and Stable Mg2+-Doped CsPbCl3Nanocrystals for Violet LEDs. J. Phys. Chem. Lett. *12*, 8203–8211. https://doi.org/10.1021/ACS.JPCLETT.1C02416/ASSET/IMAGES/LARGE/JZ1C02416_0005.JPEG.
26. Hu, M., Murrietta, N., Lyu, J., and Congreve, D.N. (2023). Two-dimensional perovskite materials towards violet and ultraviolet light-emitting diodes. In UV and Higher Energy Photonics: From Materials to Applications 2023, G. Lérondel, Y.-H. Cho, and A. Taguchi, eds. (SPIE), p. 6. https://doi.org/10.1117/12.2676613.

27. Crace, E.J., Su, A.C., and Karunadasa, H.I. (2022). Reliably obtaining white light from layered halide perovskites at room temperature. Chem. Sci. *13*, 9973–9979. https://doi.org/10.1039/D2SC02381D.

28. Han, Y., Yin, J., Cao, G., Yin, Z., Dong, Y., Chen, R., Zhang, Y., Li, N., Jin, S., Mohammed, O.F., et al. (2022). Exciton Self-Trapping for White Emission in 100-Oriented Two-Dimensional Perovskites via Halogen Substitution. ACS Energy Lett. *7*, 453–460. https://doi.org/10.1021/ACSENERGYLETT.1C02572/SUPPL_FILE/NZ1C02572_SI_002.ZIP.

29. Elleuch, S., Lusson, A., Pillet, S., Boukheddaden, K., and Abid, Y. (2020). White Light Emission from a Zero-Dimensional Lead Chloride Hybrid Material. ACS Photonics *7*, 1178–1187. https://doi.org/10.1021/ACSPHOTONICS.9B01817/SUPPL_FILE/PH9B01817_SI_001.DOCX.

30. Terashima, M., Miyayama, T., Shirao, T., Mo, H.W., Hatae, Y., Fujimoto, H., and Watanabe, K. (2020). The electronic band structure analysis of OLED device by means of in situ LEIPS and UPS combined with GCIB. Surf. Interface Anal. *52*, 948–952. https://doi.org/10.1002/SIA.6777.

31. Hikima, K., Shimizu, K., Kiuchi, H., Hinuma, Y., Suzuki, K., Hirayama, M., Matsubara, E., and Kanno, R. (2022). Operando analysis of electronic band structure in an all-solid-state thin-film battery. Commun. Chem. *5*, 52. https://doi.org/10.1038/s42004-022-00664-w.

32. Shen, Y., Shen, K.-C., Li, Y.-Q., Guo, M., Wang, J., Ye, Y., Xie, F.-M., Ren, H., Gao, X., Song, F., and Tang, J. (2021). Interfacial Potassium-Guided Grain Growth for Efficient Deep-Blue Perovskite Light-Emitting Diodes. Adv. Funct. Mater. *31*, 2006736. https://doi.org/10.1002/ADFM.202006736.

33. Zou, G., Li, Z., Chen, Z., Chu, L., Yip, H.-L., Cao, Y., Zou, G., Li, Z., Chen, Z., Chu, L., et al. (2021). Color-Stable Deep-Blue Perovskite Light-Emitting Diodes Based on Organotrichlorosilane Post-Treatment. Adv. Funct. Mater. *31*, 2103219. https://doi.org/10.1002/ADFM.202103219.

34. Yan, S., Tian, W., Chen, H., Tang, K., Lin, T., Zhong, G., Qiu, L., Pan, X., Wang, W., Yan, S., et al. (2021). Deep Blue Layered Lead Perovskite Light-Emitting Diode. Adv. Opt. Mater. *9*, 2001709. https://doi.org/10.1002/ADOM.202001709.

35. Zhang, J., Zhang, T., Ma, Z., Yuan, F., Zhou, X., Wang, H., Liu, Z., Qing, J., Chen, H., Li, X., et al. (2023). A Multifunctional "Halide-Equivalent" Anion Enabling Efficient CsPb(Br/I)3 Nanocrystals Pure-Red Light-Emitting Diodes with External Quantum Efficiency Exceeding 23. Adv. Mater. *35*, 2209002. https://doi.org/10.1002/ADMA.202209002.

36. Chen, Y., Chen, J., Zhao, Y., and Ma, D. (2012). High efficiency blue phosphorescent organic light-emitting diode based on blend of hole- and electron-transporting materials as a co-host. Appl. Phys. Lett. *100*, 213301. https://doi.org/10.1063/1.4720512/281889.

37. Su, S., Chiba, T., Takeda, T., Kido, J., Su, S., Takeda, T., Kido, J., and Chiba, T. (2008). Pyridine-Containing Triphenylbenzene Derivatives with High Electron Mobility for Highly Efficient Phosphorescent OLEDs. Adv. Mater. *20*, 2125–2130. https://doi.org/10.1002/ADMA.200701730.

38. Lee, H., Maeng, M.J., Hong, J.A., Najnin, R., Moon, J., Cho, H., Lee, J., Yu, B.G., Park, Y., and Cho, N.S. (2017). Highly efficient green, blue, and white phosphorescent inverted organic light-emitting diodes by improving charge injection and balance. J. Mater. Chem. C *5*, 9911–9919. https://doi.org/10.1039/C7TC02795H.

39. Wang, S., Wang, X., Yao, B., Zhang, B., Ding, J., Xie, Z., and Wang, L. (2015). Solution-Processed Phosphorescent Organic Light-Emitting Diodes with Ultralow Driving Voltage and Very High Power Efficiency. Sci. Rep. *5*, 12487. https://doi.org/10.1038/srep12487.

40. Wu, S., Li, S., Sun, Q., Huang, C., and Fung, M.K. (2016). Highly Efficient White Organic Light-Emitting Diodes with Ultrathin Emissive Layers and a Spacer-Free Structure. Sci. Rep. *6*, 25821. https://doi.org/10.1038/srep25821.

41. Fan, C., Zhu, L., Liu, T., Jiang, B., Ma, D., Qin, J., Yang, C., Fan, C., Liu, T., Jiang, B., et al. (2014). Using an Organic Molecule with Low Triplet Energy as a Host in a Highly Efficient Blue Electrophosphorescent Device. Angew. Chem. Int. Ed. Engl. *53*, 2147–2151. https://doi.org/10.1002/ANIE.201308046.

42. Liu, A., Bi, C., Guo, R., Zhang, M., Qu, X., Tian, J., Liu, A., Bi, C., Guo, R., Zhang, M., et al. (2021). Electroluminescence Principle and Performance Improvement of Metal Halide Perovskite Light-Emitting Diodes. Adv. Opt. Mater. *9*, 2002167. https://doi.org/10.1002/ADOM.202002167.

43. Zhao, L., Roh, K., Kacmoli, S., Al Kurdi, K., Jhulki, S., Barlow, S., Marder, S.R., Gmachl, C., Rand, B.P., Zhao, L., et al. (2020). Thermal Management Enables Bright and Stable Perovskite Light-Emitting Diodes. Adv. Mater. *32*, 2000752. https://doi.org/10.1002/ADMA.202000752.

44. Zou, C., Liu, Y., Ginger, D.S., and Lin, L.Y. (2020). Suppressing Efficiency Roll-Off at High Current Densities for Ultra-Bright Green Perovskite Light-Emitting Diodes. ACS Nano *14*, 6076–6086. https://doi.org/10.1021/ACSNANO.0C01817/ASSET/IMAGES/LARGE/NN0C01817_0005.JPEG.

45. Zhao, B., Guo, B., Xing, S., Liu, Z., Yuan, Y., Ren, Z., Tang, W., Lian, Y., Zhang, G., Zou, C., and Di, D. (2024). Highly stable perovskite light-emitting diodes. Matter *7*, 772–793. https://doi.org/10.1016/J.MATT.2023.11.022.